Phonon dispersion in WS_2

To cite this article: S M Souliou *et al* 2025 *2D Mater.* **12** 045012

2D Materials

PAPER

Phonon dispersion in WS_2

S M Souliou[1,2,10,*], H Tornatzky[3,4,10,*], R Gillen[5,6,*], S Kuffer[5], A Michail[7,8], J Parthenios[7], A Bosak[2], L Paolasini[2], J Maultzsch[5] and K Papagelis[9]

[1] Institute for Quantum Materials and Technologies, Karlsruhe Institute of Technology, Kaiserstr. 12, 76021 Karlsruhe, Germany
[2] ESRF, The European Synchrotron, 71, avenue des Martyrs, CS 40220, F-38043 Grenoble Cedex 9, France
[3] Institut für Festkörperphysik, Technische Universität Berlin, Hardenbergstraße 36, 10623 Berlin, Germany
[4] PDI, Paul-Drude-Institut für Festkörperelektronik, Leibniz-Institut im Forschungsverbund Berlin e.V., Hausvogteiplatz 5–7, 10117 Berlin, Germany
[5] Department of Physics, Friedrich-Alexander-Universität Erlangen-Nürnberg, 91058 Erlangen-Nürnberg, Germany
[6] College of Engineering, Swansea University, SA1 8EN Swansea, United Kingdom
[7] Institute of Chemical Engineering Sciences, Foundation of Research and Technology-Hellas (FORTH/ICEHT), 26504 Patras, Greece
[8] Department of Physics, University of Patras, 26504 Patras, Greece
[9] School of Physics, Department of Solid State Physics, Aristotle University of Thessaloniki, 54124 Thessaloniki, Greece
[10] These authors contributed equally to this work.
[*] Authors to whom any correspondence should be addressed.

E-mail: michaela.souliou@kit.edu, ht07@physik.tu-berlin.de and roland.gillen@fau.de

Keywords: WS_2, transition metal dichalcogenides, phonons, inelastic x-ray scattering, density functional perturbation theory

Supplementary material for this article is available online

OPEN ACCESS

RECEIVED
20 May 2025

REVISED
1 August 2025

ACCEPTED FOR PUBLICATION
22 August 2025

PUBLISHED
17 September 2025

Abstract

We present a combined experimental and theoretical study of the phonon dispersion in bulk 2H-WS_2 by means of inelastic x-ray scattering and density functional perturbation theory. Our findings highlight the two-dimensional character of the lattice dynamics in this van-der-Waals system and indicate the significance of the bulk phonon measurements for the monolayer counterpart. The agreement between the simulated phonon scattering factors and the experimentally measured phonon spectra allow to map an extensive part of the phonon dispersion curves along high-symmetry crystallographic directions and serve as a reference for future experiments under variable experimental conditions.

1. Introduction

Transition metal dichalcogenides (TMDCs) comprise a relatively old class of layered compounds [1, 2], recently revitalized by the isolation of two-dimensional (2D) materials from their bulk counterparts [3–9]. Among them, tungsten disulfide (WS_2) compiles a list of interesting physical properties, including a sizeable direct electronic band gap (∼2.1 eV), a high photoluminescence quantum yield (6%), and intrinsically large exciton and trion binding energies [10]. Moreover, the significant spin–orbit splitting (0.3–0.7 eV) of the symmetry inequivalent valleys at the K and K′ points of its Brillouin zone, lead to an effectively large spin–valley coupling [11]. These attributes make WS_2 particularly attractive for a variety of applications such as optoelectronic [12–15], tribological [16, 17], triboelectric [18], catalytic [19], valleytronics [20] applications and energy harvesting [21], rendering it one of the most studied TMDC compounds.

The performance of WS_2-based devices is strongly influenced by its lattice dynamics, as phonons govern many key physical properties of 2D materials. In semiconducting or insulating 2D systems in particular, thermal conduction is primarily determined by phonon transport, with heat flow limited by phonon–phonon interactions such as anharmonic scattering [22, 23]. Additionally, it has been highlighted that understanding and engineering the phonon spectrum of such systems could facilitate control over sound and heat across relevant frequencies, enabling the design and fabrication of novel phononic crystals and devices that harness heat conduction rather than conventional electrical properties [24]. A detailed characterization of the phonon spectrum is therefore essential for understanding the intrinsic thermal transport mechanisms in WS_2.

Up to date, experimental investigations of the phonons in WS_2 and in other 2D TMDCs, are primarily conducted using Raman spectroscopy. It is worth noting that surface-sensitive techniques—such as high-resolution electron energy loss spectroscopy and helium atom scattering—have been successfully employed in other TMDCs and 2D materials to probe surface phonon dispersions, offering valuable insights into the surface-localized character of vibrational modes and phonon confinement effects [25–27]. In WS_2, the first-order Raman spectrum reveals details, such as the number of layers, the mechanical strain, and doping [28–30].

Despite being a very powerful technique, Raman scattering is typically limited to excitations close to the center of the Brillouin zone, thus failing to provide information on the dispersion of the phononic excitations. Recent works have explored the very rich second- and higher-order Raman spectrum of WS_2 by tuning the excitation energy near excitonic transitions [28, 31, 32]. The observed Raman features were attributed to difference, combination and defect-activated modes, induced by double resonance Raman processes [33, 34]. Although this technique is widely used to investigate electron-phonon scattering pathways in 2D TMDCs systems — for example, unveiling the physics of intervalley scattering by acoustic phonons [35] and probing the valence band spin–orbit splitting by electron–two phonon triple–resonance scattering processes [36]—the interpretation of many of the higher order features observed in the Raman spectra remains open.

It is, therefore, of high importance to obtain direct experimental input on the phonon dispersion curves of WS_2. However, while computational phonon studies of bulk and monolayer systems are available in the literature [33, 37], experimental data remain limited to a few low-energy phonon branches from older inelastic neutron scattering (INS) studies [38, 39]. Here, we report on the phonon dispersion in 2H-WS_2 measured along the main high-symmetry directions of the Brillouin zone using high-resolution inelastic x-ray scattering (IXS) on single crystals. Our experimental results underline the 2D character of the phonon dispersion in WS_2 and show very good agreement with the results of density functional perturbation theory calculations, particularly when combining the local-density approximation with explicit inclusion of spin–orbit interaction. The precise simulation of the structure factors of the measured phonon spectra sets the framework for targeted studies of specific phonon branches under varying temperature, pressure, or strain in TMDC thin films.

2. Methods

2.1. Experimental methods

High-quality single crystals of 2H-WS_2 were purchased from HQ graphene, Netherlands. For the IXS measurements, a thin flake was exfoliated from a single crystal piece. The thickness of the measured sample ($\sim$25 μm) was close to the absorption length at the incident x-ray energy, allowing measurements in transmission geometry.

The IXS experiments were performed at the ID28 beamline at the European Synchrotron Radiation Facility [40]. The incident photon energy was 17.794 keV, and the corresponding instrumental energy resolution was 3 meV (full width at half maximum). The x-ray beam was focused by multilayer mirrors to a 25 $\times$ 25 μm spot (horizontally $\times$ vertically) on the sample surface. Energy scans were collected at constant momentum transfers, selected by the scattering angle and the sample orientation. The scattered photons were analyzed by a set of 9 crystal analyzers placed at the end of a 7 m long arm. IXS scans including the quasi-elastic line or at least one peak originated by anti-Stokes scattering were regularly recorded throughout the experiment to calibrate the energy scale. The momentum resolution was set to $\sim$0.25 nm^{-1} in the scattering plane and 0.75 nm^{-1} perpendicular to it. In the following, the momentum transfers are given in reciprocal lattice units (r.l.u.) of the hexagonal unit cell. All measurements were conducted at ambient conditions. The experimental phonon spectra were fitted using damped harmonic oscillator functions convoluted with the instrumental resolution. Based on the results of these fits we have experimentally derived the phonon dispersion.

2.2. Computational methods

We used the Quantum Espresso code to perform density functional theory (DFT) simulations of the theoretical phonon dispersion curves of bulk WS_2 [41–43]. The DFT simulations closely followed the computational approach reported in [44], with an increased cutoff energy of 135 Ry. We performed two sets of simulations: one set using the PBE exchange-correlation functional with D3 dispersion corrections (PBE-D3) [44–46], without inclusion of spin–orbit interaction. As a second approach, we computed the phonon dispersion using the LDA exchange-correlation and explicitly including spin–orbit interaction in all parts of the simulations (LDA + SOI).

3. Results and discussion

2H-WS_2 crystallizes in a hexagonal structure (space group $P6_3/mmc$, No. 194), composed of weakly-bonded single layers of S–W–S, in a 2H stacking order along the c-axis [47]. Each single layer includes a trigonal prismatic arrangement of two planes of S atoms and an intercalated plane of W atoms. The hexagonal unit cell of the bulk material contains six atoms, giving rise to 18 phonon branches. Figure 1 presents the DFPT calculated dispersion along the high-symmetry directions of the reciprocal space, namely Γ–M, Γ–K, K–M, and Γ–A. A sketch of the first Brillouin zone

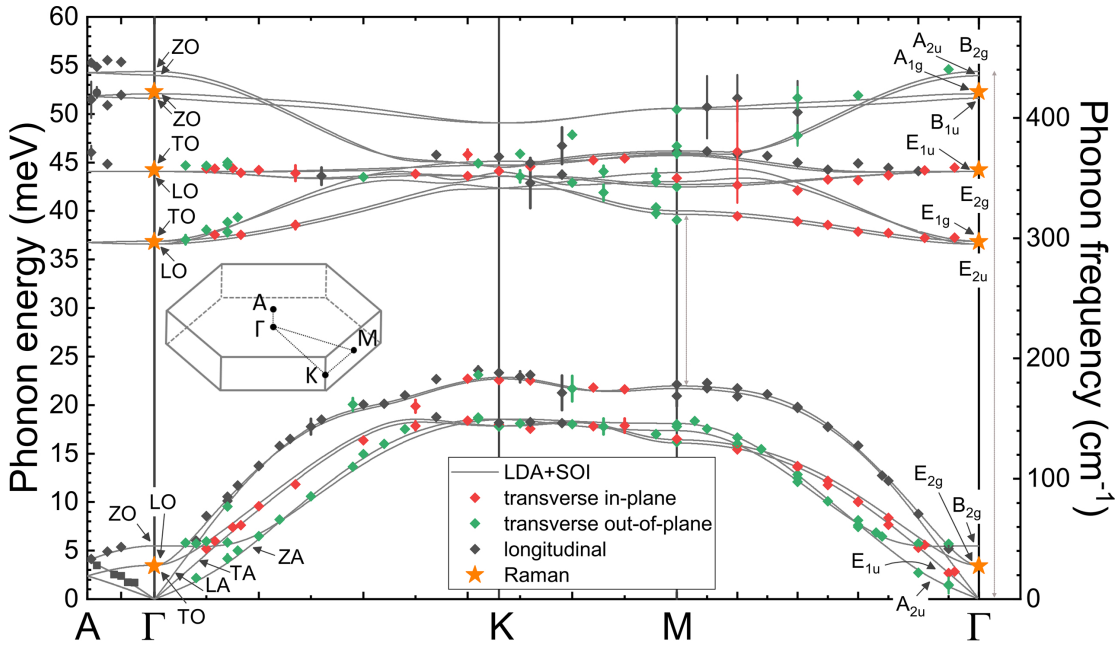

Figure 1. The phonon dispersion of WS_2 along the high-symmetry directions A–Γ–K–M–Γ. Solid symbols correspond to the results of IXS experiments, whereas the solid lines show the DFPT calculations using the LDA + SOI approach. Grey/red/green symbols indicate measurements performed in predominantly longitudinal/TIP/TOP geometries close to the Γ point (see main text), respectively. Measurements were often performed at reciprocal space positions extending over a range of out-of-plane l components (see supplemental material for more information on the l dependence of the phonon dispersion curves). Some of the TIP measurements were performed with a small experimental offset from the Γ–M and Γ–K–M paths (see supplemental material). The orange star symbols correspond to Raman data collected on the studied WS_2 crystal and Raman data available in the literature [30, 48, 49]. The dotted gray arrowed lines indicate the overall phonon bandwidth (∼55 meV) and the gap at the M point (∼20 meV).

and its high-symmetry points is also given in the inset of figure 1.

IXS spectra measured at various wavevectors along the Γ–M direction are presented in figure 2. In IXS experiments, the measured intensity depends on the total momentum transfer $\boldsymbol{Q} = \boldsymbol{q} + \boldsymbol{G}_{\mathrm{HKL}}$ where $\boldsymbol{G}_{\mathrm{HKL}}$ is the Brillouin zone center closest to $\boldsymbol{Q}$, and $\boldsymbol{q}$ is the reduced momentum transfer [50]. The spectra presented in figure 2 were measured in Brillouin zones near the G_{200} = (2 0 0), G_{110} = (1 1 0) and G_{0010} = (0 0 10) Bragg peaks and along Γ–M direction. The low-energy IXS intensity comes mainly from the longitudinal acoustic, the transverse in-plane (TIP) acoustic, and the transverse out-of-plane (TOP) acoustic branch, respectively (see supplemental material for details on additional contributions from the structure factor calculations). Inelastic signal at negative ΔE corresponds to the anti-Stokes scattering process, i.e. the annihilation of phonons. We note that the small—or even absent—quasi-elastic line in the measured spectra (away from the Bragg peaks) indicates the high quality of the measured crystal [51, 52].

The IXS experiments were conducted in several Brillouin zones, chosen based on the dynamical structure factor calculations, allowing us to measure the dispersion of the acoustic and most optical phonon branches along main crystallographic directions. An overview of the experimentally determined phonon dispersion, obtained after fitting the IXS spectra, is given in figure 1, overlaid with the DFPT calculations. The IXS data were collected in longitudinal, TIP, and TOP geometries, although mixed geometries were often used to benefit from increased structure factors. In such cases, the dominant character of the scattering geometry (close to the Γ point) is shown in figure 1. We also note that some of the spectra (particularly along the Γ–K–M directions) were measured at reciprocal space positions extending over a range of out-of-plane l components (see SM for more information on the l dependence of the phonon dispersion curves). Phonon energies at the Γ point obtained from Raman measurements are also included in figure 1 [30, 48, 49].

The overall phonon bandwidth is close to ∼55 meV. The lower energy phonon branches are separated from the higher energy ones by a 20 meV gap at the M point, which is much larger than the ∼10 meV gap in isostructural MoS_2 and WSe_2 [44, 53]. This significantly increased phonon gap was indicated by earlier phonon dispersion calculations—and was shown to be also relevant for monolayers, as will be discussed next—and was linked to reduced phonon-phonon scattering rates in three-phonon

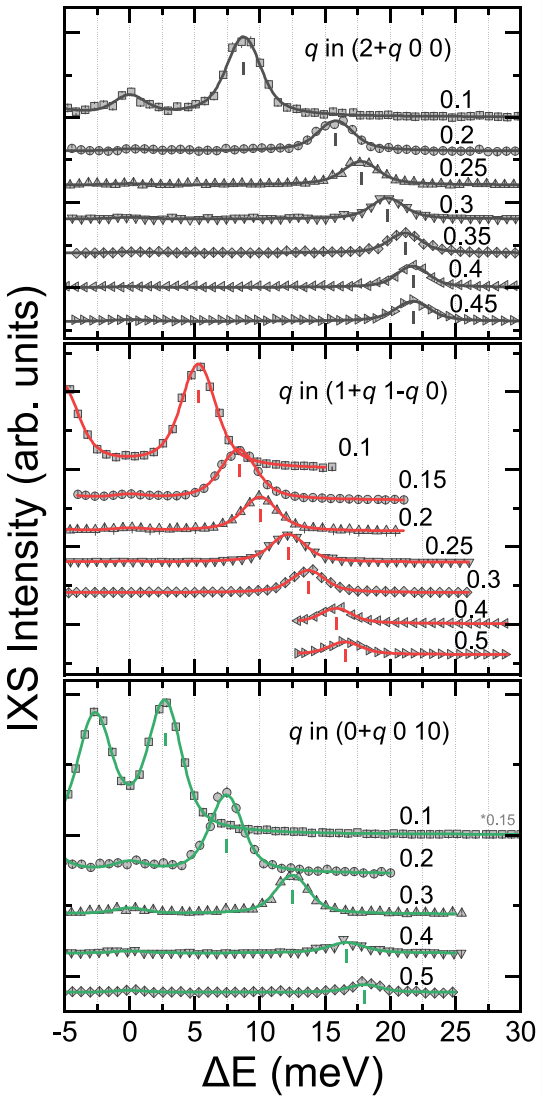

Figure 2. Experimental IXS spectra of WS_2 recorded along the Γ–M direction close to the G_{200}, G_{110}, and G_{0010} Brillouin zones. Some of the measurements close to G_{200} were performed at reciprocal space positions extending over a short range of *l*. The spectra are vertically shifted for clarity. Thick solid lines correspond to data fits, and vertical tick marks represent phonon energies extracted from the data fitting.

processes [54]. As indicated in figure 1, the modes at the zone center belong to the following irreducible representations [28, 55]:

$$\Gamma = A_{1g} + 2B_{2g} + E_{1g} + 2E_{2g} + 2A_{2u} + B_{1u} + 2E_{1u} + E_{2u}.$$

In agreement with earlier calculations [33, 37], the phonons disperse from Γ along the main directions of the first Brillouin zone in nearly doubly degenerate pairs of branches, known as Davydov pairs. In each pair, one branch corresponds to in-phase atomic vibrations on neighboring layers in the bulk unit cell, while the other exhibits vibrations in antiphase [37, 56]. While this splitting is absent in monolayer WS_2, it is a signature of the interlayer interaction in multilayer and bulk systems. The weak van der Waals interactions in WS_2 (similar to other TMDCs) result in a minimal splitting for the higher energy optical phonon branches—approximately ∼1 meV at its maximum value according to our calculations—which cannot be unambiguously resolved within the energy resolution of the IXS experiment.

At lower energies, each acoustic phonon branch is paired with a low-energy optical phonon branch of finite phonon energy at the Γ point, namely the twofold degenerate Raman active in-plane rigid layer shear modes with E_{2g} symmetry and the out-of-plane rigid layer breathing mode with B_{2g} symmetry. These low-energy optical modes have attracted attention for their high sensitivity to layer number, interlayer coupling and stacking [57]. Near the zone center, the optical branches exhibit a sizable energy splitting to their paired acoustic branches (∼3.5 meV for shear modes and ∼5.5 meV for breathing modes), which diminishes at higher momentum transfers. In our IXS experiments, we observed individual branches of paired modes close to the Γ point exploiting the enhancement of the structure factor of one of the two modes of the pair at selected Brillouin zones. This is illustrated in figure 3 for the case of the B_{2g} mode's branch, which, in excellent agreement with our simulations, has an enhanced contribution close to Bragg peaks with odd *L* values ($L = 11$, shown in figure 3). Its acoustic pair, namely the TOP acoustic branch (commonly referred to as the flexural mode, ZA in figure 1), dominates the spectra measured close to even *L* values ($L = 10$, shown in figures 2 and A2 in the SM), consistent also with the presence of a strong Bragg peak at $L = 10$. This behavior can be explained by the atomic structure of the system and the contribution of the individual species to the IXS scattering: for acoustic phonon modes, mainly the heavy tungsten atoms contribute, which form two sublayers spaced by half the out-of-plane lattice constant *c*. For even *L* values, the scattering from the vibrating individual tungsten layers interferes constructively for the TOP acoustic mode (atoms moving in phase) and destructively for the TOP optical mode, leading to a large IXS structure factor for the acoustic mode. For odd L values, the situation is reversed due to a 180° phase difference between the scattered waves from the two individual layers, and the IXS signal of the TOP optical mode is enhanced compared to that of the TOP acoustic mode.

The phonon energies of the low-energy longitudinal and TIP acoustic branches along the Γ–M direction (with an exception at the M point) align closely with those reported earlier from INS measurements, while greater deviations are observed along the Γ–K direction [38]. This could possibly originate from the

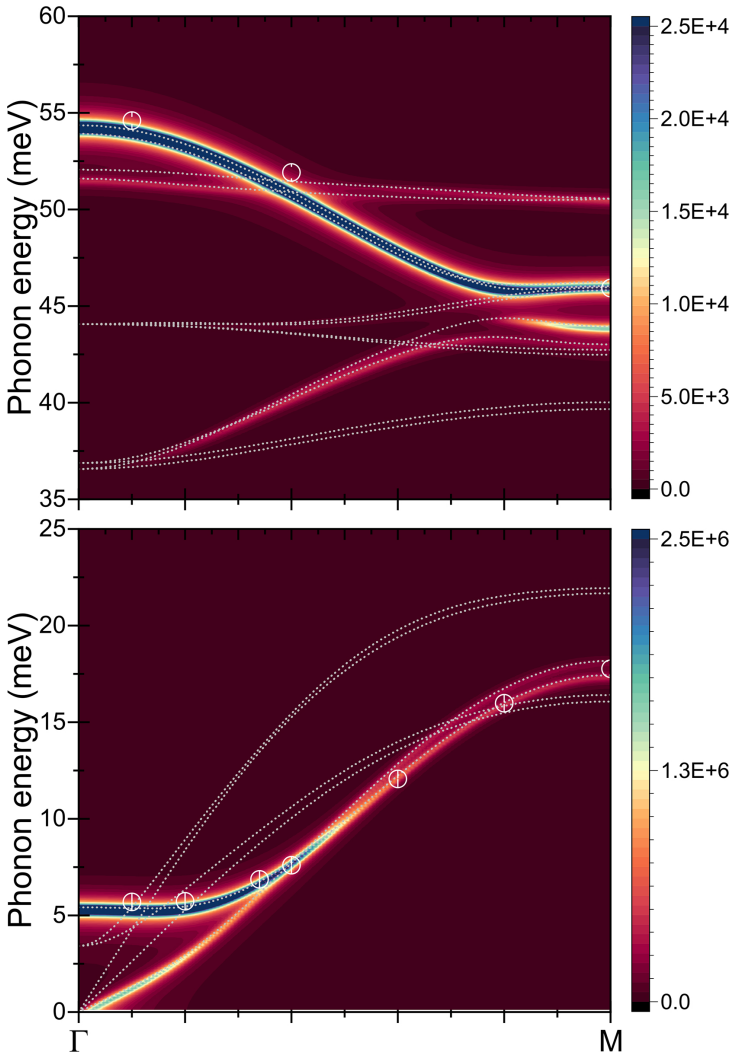

Figure 3. Colormap of the simulated dynamical structure factors along the Γ–M direction close to G_{0011} = (0 0 11) and the relevant experimentally determined dispersion derived from fitting the IXS data (white symbols). The dashed gray lines represent the LDA + SOI calculated dispersion of all the phonon branches.

different scattering volumes employed in IXS and INS experiments.

The overall relatively weak l dependence of the phonon dispersion curves (except for the lowest energy branches close to the zone center—see figure A4 in SM) highlights the quasi-2D nature of the lattice dynamics in this bulk material. This is further corroborated by the almost quadratic dispersion of the flexural phonon branch (ZA) close to the Γ point, a behavior typically encountered in 2D systems [58] which was previously observed experimentally, amongst others, in graphite [59], bulk WSe_2 [53] and MoS_2 [44] and exploited to derive further material properties such as the bending rigidity [60, 61]. This is also in line with earlier computational studies on monolayer and bulk WS_2 and MoS_2, which showed that—apart from the rigid-layer modes near the Γ point—the vibrational properties of monolayers bear a strong resemblance to those of the bilayers and bulk [37, 62]. This is in stark contrast with the electronic band structure of WS_2, which undergoes a significant change from the monolayer to the multilayer system, resulting in a direct to indirect bandgap transition [33]. Notably, unlike the case of other dichalcogenides for which the calculations slightly overestimate the flexural branch energy [44, 53], the phonon calculations presented here show a very good agreement with the experimental ZA branch values of WS_2. For the LDA calculations, the ZA branch shows the expected quadratic dispersion typical for 2D systems, while the inclusion of spin–orbit interaction leads to a slightly larger quadraticity compared to a reference LDA simulation without spin–orbit interaction (see figure 5). In the PBE-D3 simulations, the ZA branch displays a more linear dispersion, indicative of bulk-like systems and consistent with our previous study on bulk MoS_2 [44].

Interestingly, a recent IXS study on the sibling compound WSe_2 identified a low-temperature softening of this branch close to the zone center, associating this behavior with an increased stiffness towards flexural vibrations at higher temperatures,

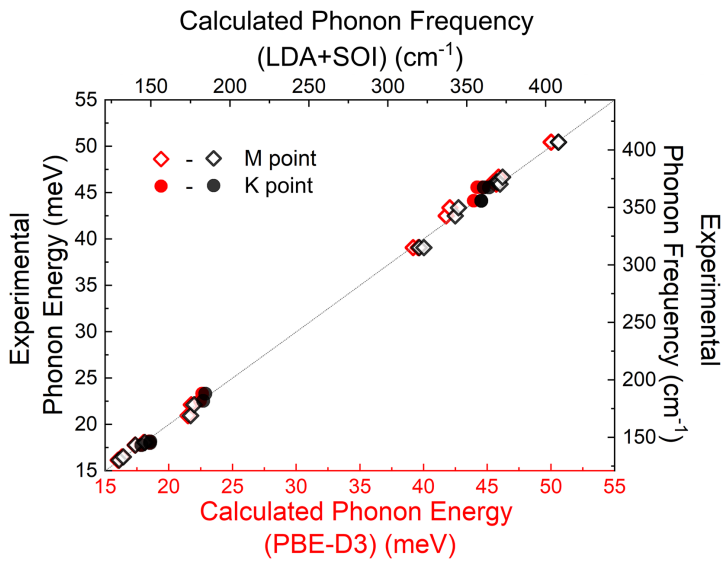

Figure 4. Comparison of the experimentally determined phonon frequencies at the M and K points of the Brillouin zone with those obtained from PBE-D3 and LDA + SOI calculations. A detailed comparison can be found in table A1 in the SM.

which further indicates weak interlayer interactions [53]. On the other hand, high-pressure studies of WS_2 and other TMDCs [63, 64] found evidence for a semiconductor-to-metal transition as the interlayer distance decreases under pressure. Future temperature- and pressure- dependent IXS measurements on WS_2 and other TMDCs would clarify whether the low-temperature behavior of the ZA branch is a characteristic feature within the family and would elucidate how the lattice dynamics (in particular, the ZA and rigid layer branches) behave as the system becomes more 3D-like in the high-pressure metallic state.

Based on the experimentally measured dispersion, and incorporating the DFPT-derived results, we calculated the speed of sound in WS_2. Specifically, we fit the slope of the branch associated with the LA phonon at the Γ point, obtaining a speed of sound of 1.0 km s^{-1} along both the ΓM and ΓK directions. This value is of comparable order, yet slower than previous estimates, namely 4.6 km s^{-1} using DFPT [65] or 2.8 km s^{-1} derived from elastic constants [66].

Finally, regarding the high-energy optical phonon branches, the dispersion of most of them were experimentally observed in good agreement with the calculations (for the highest energy branch along the Γ–K–M directions, see SM). The phonon frequencies at the M and K points, which are particularly important for the interpretation of higher-order features observed in Raman spectra [28], are presented in figure 4. The PBE-D3 and the LDA + SOI approaches give comparable results for the low-energy modes. For the higher energy branches, there is an overall better agreement of the LDA + SOI results to the frequencies determined by IXS, within experimental error. We note that in general, the quantitative reproduction of phonon dispersion in van-der-Waals materials using DFT is somewhat challenging. The widely used exchange-correlation functional PBE tends to exhibit a systematic 'underbinding,' an underestimation of interatomic bonding strength. Consequently, the lattice constants are overestimated and the phonon frequencies generally underestimated (see table 1). This underestimation is particularly pronounced for the soft shear and breathing modes, for which the layers move rigidly and the frequency is determined by the weak interlayer forces. Our simulations confirm that this flaw can be overcome through the inclusion of van-der-Waals corrections, which complement the artificially short-range non-covalent interaction in the PBE approximation. This has a beneficial effect on both the in-plane and out-of-plane lattice constants and introduces a hardening of the phonon frequencies, showing improved agreement with experimental values. These benefits of including van-der-Waals interaction effects in phonon simulations on low-dimensional and layered materials have been widely recognized and discussed, e.g. for graphite [67], bulk MoS_2 [44], Bi_2Te_3 (111) surfaces [27], and bulk $CrCl_3$ [68]. On the other hand, our simulations on bulk WS_2 and MoS_2 [44] exhibit a distinct linearity for the ZA branch close to the Brillouin zone center. For small wavevectors, the frequency of the ZA mode in layered materials is determined by subtle interatomic forces and typically is very sensitive to the quality of the DFT-derived groundstate electron density and atomic structure. The long-range interlayer coupling due to the inclusion of van-der-Waals corrections might lead to a slightly increased

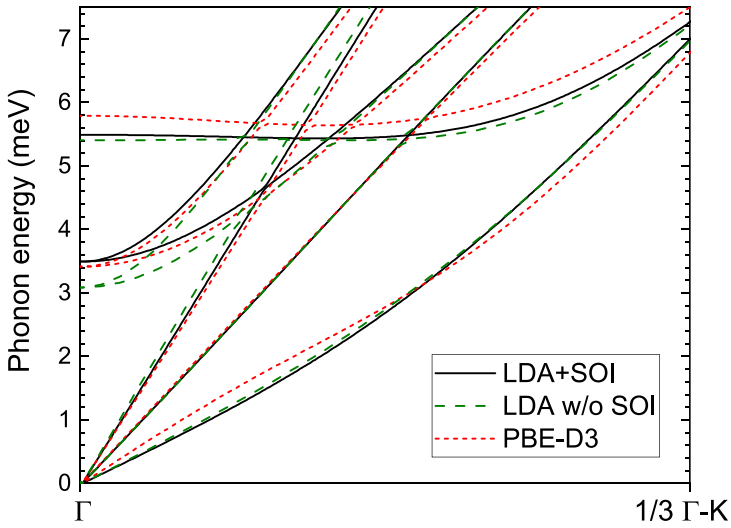

Figure 5. Comparison of the dispersion of low-energy phonon modes computed by the LDA + SOI (black solid lines) and PBE-D3 (red dashed lines) approaches. For reference, results from LDA simulations without spin–orbit coupling are also included (green dashed lines). LDA + SOI predicts a slightly more pronounced quadratic dispersion for the ZA branch compared to PBE-D3.

Table 1. Comparison of lattice constants and phonon frequencies obtained for different DFT calculations with and without inclusion of spin–orbit interaction and van-der-Waals corrections. Two representative phonon modes at the Brillouin center were chosen: 1. The low-frequency shear (E_{2g}) mode, which is defined by interlayer interaction. 2. The high-frequency A_{1g} mode prominent in Raman spectra, which is defined by intralayer interactions.

			Representative phonons (cm^{-1})	
Theory level	a (Å)	c (Å)	Shear	A_{1g}
LDA w/o SOI	3.131	12.173	24.9	421.8
LDA w/o SOI (LDA + SOI lattice constants)			25.1	421.8
LDA + SOI	3.133	12.163	27.6	419.8
PBE	3.188	14.755	11.3	406.8
PBE-D3	3.163	12.296	27.5	417.7
Exp.	3.153[a]	12.323[a]	28[b]	420[b]

[a] Berkdemir *et al*[33].

[b] Raman measurements on the measured sample and from the literature [30, 48, 49].

bulk-like nature of the lattice vibrations, which particularly affects the sensitive ZA branch.

Conversely, LDA exchange-correlation functionals suffer from systematic 'overbinding', which often results in a rather fortuitous agreement with experimental results. In the case of MoS_2 and WS_2, LDA (without SOI) provides a good quantitative description of the phonon frequencies, albeit with a slight overestimation for the high-energy modes. In contrast to PBE-D3, the interatomic interaction potential in LDA rapidly decays with distance, which, e.g. causes the well-known underestimated evolution of the interlayer binding energy of graphite with interlayer distance [69]. This might contribute to the predicted quadratic dispersion of the ZA mode, as LDA mainly couples neighboring layers, while the mid- and long-distance interlayer coupling vanishes. Our simulations in the present work further reveal that the inclusion of SOI slightly softens the high-energy phonon modes and hardens the low-energy modes (see figure 5). For the high-energy optical phonon branches, we generally find that the LDA + SOI frequencies are about 1 meV higher than those obtained from our PBE-D3 simulations and are in better agreement with our IXS measurements (see figure 1). This improvement can partially be attributed to a 'volume effect' stemming from small SOI-induced adjustments of the interatomic interaction: We find that SOI reduces the overbinding for the covalent bonds inside each layer, resulting in a slightly larger in-plane lattice constant (see table 1). In out-of-plane direction, the lattice constant is slightly decreased by 0.1%. These adjustments can be understood as a softening (hardening) of the intralayer (interlayer) interatomic 'spring constants', hence causing, e.g. a downshift of the high-energy modes, the frequency of which is

defined by the strength of intralayer atomic bonds. Similar trends were recently reported for simulations on Bi_2Te_3 [27], where SOI effects are expected to be strong due to the heavy atoms in the compound, and also for bulk $CrCl_3$ [68].

To obtain additional insights into the effect of the inclusion of spin–orbit interaction on the phonon mode frequencies, we calculated the vibrational spectrum at the Brillouin zone center on the level of LDA without SOI, but using the LDA + SOI lattice constants. This approach maintains the volume effect but removes other contributions from SOI on the electronic structure, for example when the perturbation theory is used to calculate the phonons. Our simulations suggest that only about 6% of the SOI-induced frequency shifts for the lowest and highest energy phonons arise from the pure volume effect. This highlights the importance of proper inclusion of the subtle interplay of non-covalent interlayer coupling and spin–orbit interactions for the phonon spectrum of WS_2.

4. Summary and outlook

We have performed a comprehensive study of the phonon dispersion in WS_2 employing IXS experiments and DFPT calculations. Our data demonstrate the predominantly 2D character of the phonons in this layered material and highlight the relevance of this study for its monolayer counterpart. The good agreement between the experimental and computational results further validates the accuracy of the density functional perturbation theory calculations, particularly concerning other members of the TMDC family for which experimental phonon dispersion data are currently lacking. Finally, the presented IXS data, which cover most of the phonon branches, and the successful simulation of the measured structure factors serve as a reference for future targeted experimental studies of specific phonon branches under various experimental conditions, such as low temperatures, high pressures, or grazing incidence conditions on TMDCs thin films [70, 71].

Data availability statement

The data that support the findings of this study are available upon reasonable request from the authors.

Acknowledgments

S M S and H T contributed equally to this work. S M S acknowledges funding by the Deutsche Forschungsgemeinschaft (DFG, German Research Foundation)—Projektnummer 441231589. The authors gratefully acknowledge the scientific support and HPC resources provided by the Erlangen National High Performance Computing Center (NHR@FAU) of the Friedrich-Alexander-Universität Erlangen-Nürnberg (FAU) under the NHR project #b181dc. NHR funding is provided by federal and Bavarian state authorities. NHR@FAU hardware is partially funded by the German Research Foundation (DFG)—440719683. We acknowledge the European Synchrotron Radiation Facility (ESRF) for provision of synchrotron radiation facilities under proposal number HC-4047. We thank Aren Yazmaciyan for careful reading of the manuscript.

Author contributions

S M Souliou 0000-0001-9201-7392
Conceptualization (equal), Data curation (equal), Formal analysis (equal), Funding acquisition (equal), Investigation (equal), Methodology (equal), Project administration (equal), Resources (equal), Validation (equal), Visualization (equal), Writing – original draft (equal), Writing – review & editing (equal)

H Tornatzky 0000-0002-3153-0501
Conceptualization (equal), Data curation (equal), Formal analysis (equal), Funding acquisition (equal), Investigation (equal), Methodology (equal), Project administration (equal), Resources (equal), Software (equal), Validation (equal), Visualization (equal), Writing – review & editing (equal)

R Gillen 0000-0002-7913-0953
Data curation (equal), Formal analysis (equal), Investigation (equal), Methodology (equal), Software (equal), Supervision (equal), Validation (equal), Visualization (equal), Writing – original draft (equal), Writing – review & editing (equal)

S Kuffer 0009-0000-2339-1188
Formal analysis (supporting), Investigation (supporting), Software (supporting)

J Parthenios
Data curation (supporting), Funding acquisition (supporting), Investigation (supporting), Writing – review & editing (equal)

A Bosak 0000-0001-8199-2301
Investigation (supporting), Methodology (supporting)

L Paolasini 0000-0003-2699-7200
Investigation (supporting), Methodology (supporting)

J Maultzsch 0000-0002-6088-2442
Conceptualization (supporting), Funding acquisition (supporting), Resources (supporting), Supervision (equal), Validation (equal), Writing – review & editing (equal)

K Papagelis 0000-0001-5094-9837
Conceptualization (equal), Data curation (supporting), Funding acquisition (equal), Investigation (supporting), Supervision (equal), Validation (supporting), Writing – original draft (supporting), Writing – review & editing (supporting)

References

[1] Dickinson R G and Pauling L 1923 *J. Am. Chem. Soc.* **45** 1466
[2] Wilson J A and Yoffe A D 1969 *Adv. Phys.* **18** 193
[3] Akinwande D *et al* 2017 *Extreme Mech. Lett.* **13** 42–77
[4] Butler S Z *et al* 2013 *ACS Nano* **7** 2898
[5] Das S, Robinson J A, Dubey M, Terrones H and Terrones M 2015 *Annu. Rev. Mater. Res.* **45** 1
[6] Wang F *et al* 2018 *Chem. Soc. Rev.* **47** 6296
[7] Mak K F, Lee C, Hone J, Shan J and Heinz T F 2010 *Phys. Rev. Lett.* **105** 136805
[8] Splendiani A, Sun L, Zhang Y, Li T, Kim J, Chim C-Y, Galli G and Wang F 2010 *Nano Lett.* **10** 1271
[9] Radisavljevic B, Radenovic A, Brivio J, Giacometti V and Kis A 2011 *Nat. Nanotechnol.* **6** 147
[10] Schaibley J R, Yu H, Clark G, Rivera P, Ross J S, Seyler K L, Yao W and Xu X 2016 *Nat. Rev. Mater.* **1** 16055
[11] Zhao S, Li X, Dong B, Wang H, Wang H, Zhang Y, Han Z and Zhang H 2021 *Rep. Prog. Phys.* **84** 026401
[12] Muoi D, Hieu N N, Phung H T T, Phuc H V, Amin B, Hoi B D, Hieu N V, Nhan L C, Nguyen C V and Le P T T 2019 *Chem. Phys.* **519** 69
[13] Chernikov A, van der Zande A M, Hill H M, Rigosi A F, Velauthapillai A, Hone J and Heinz T F 2015 *Phys. Rev. Lett.* **115** 126802
[14] Ye Z, Cao T, O'Brien K, Zhu H, Yin X, Wang Y, Louie S G and Zhang X 2014 *Nature* **513** 214
[15] Yuan L and Huang L 2015 *Nanoscale* **7** 7402
[16] Kobayashi Y, Taniguchi T, Watanabe K, Maniwa Y and Miyata Y 2017 *Appl. Phys. Express* **10** 045201
[17] Büch H, Rossi A, Forti S, Convertino D, Tozzini V and Coletti C 2018 *Nano Res.* **11** 5946
[18] Wang H, Huang C-C and Polcar T 2019 *Sci. Rep.* **9** 12570
[19] Fu Q, Yang L, Wang W, Han A, Huang J, Du P, Fan Z, Zhang J and Xiang B 2015 *Adv. Mater.* **27** 4732
[20] Ahn E C 2020 *npj 2D Mater. Appl.* **4** 17
[21] Bin Rafiq M K S, Amin N, Alharbi H F, Luqman M, Ayob A, Alharthi Y S, Alharthi N H, Bais B and Akhtaruzzaman M 2020 *Sci. Rep.* **10** 771
[22] Gu X, Wei Y, Yin X, Li B and Yang R 2018 *Rev. Mod. Phys.* **90** 041002
[23] Carvalho B R and Pimenta M A 2020 *2D Mater.* **7** 042001
[24] Balandin A A 2020 *ACS Nano* **14** 5170
[25] Brusdeylins G, Heimlich C, Skofronick J G, Toennies J P, Vollmer R, Benedek G and Miglio L 1990 *Phys. Rev. B* **41** 5707
[26] Maier P, Hourigan N J, Ruckhofer A, Bremholm M and Tamtögl A 2023 *Front. Chem.* **11** 1249290
[27] Tamtögl A *et al* 2018 *Nanoscale* **10** 14627
[28] Zhang X, Qiao X-F, Shi W, Wu J-B, Jiang D-S and Tan P-H 2015 *Chem. Soc. Rev.* **44** 2757
[29] Kolesnichenko P V, Zhang Q, Yun T, Zheng C, Fuhrer M S and Davis J A 2020 *2D Mater.* **7** 025008
[30] Michail A, Anestopoulos D, Delikoukos N, Grammatikopoulos S, Tsirkas S A, Lathiotakis N N, Frank O, Filintoglou K, Parthenios J and Papagelis K 2023 *J. Phys. Chem. C* **127** 3506
[31] Molas M R, Nogajewski K, Potemski M and Babiński A 2017 *Sci. Rep.* **7** 5036
[32] Liu H-L *et al* 2018 *Sci. Rep.* **8** 11398
[33] Berkdemir A *et al* 2013 *Sci. Rep.* **3** 1755
[34] Gaur A P S, Sahoo S, Scott J F and Katiyar R S 2015 *J. Phys. Chem. C* **119** 5146
[35] Carvalho B R, Wang Y, Mignuzzi S, Roy D, Terrones M, Fantini C, Crespi V H, Malard L M and Pimenta M A 2017 *Nat. Commun.* **8** 14670
[36] Sun L *et al* 2013 *Phys. Rev. Lett.* **111** 126801
[37] Molina-Sánchez A and Wirtz L 2011 *Phys. Rev. B* **84** 155413
[38] Sourisseau C, Fouassier M, Alba M, Ghorayeb A and Gorochov O 1989 *Mater. Sci. Eng. B* **3** 119
[39] Sourisseau C, Cruege F, Fouassier M and Alba M 1991 *Chem. Phys.* **150** 281
[40] Krisch M and Sette F 2007 *Light Scattering in Solid IX* ed M Cardona and R Merlin (Springer) p 317
[41] Giannozzi P *et al* 2009 *J. Phys.: Condens. Matter* **21** 395502
[42] Hamann D R 2013 *Phys. Rev. B* **88** 085117
[43] van Setten M J, Giantomassi M, Bousquet E, Verstraete M J, Hamann D R, Gonze X and Rignanese G-M 2018 *Comput. Phys. Commun.* **226** 39
[44] Tornatzky H, Gillen R, Uchiyama H and Maultzsch J 2019 *Phys. Rev. B* **99** 144309
[45] Grimme S, Ehrlich S and Goerigk L 2011 *J. Comput. Chem.* **32** 1456
[46] Tyborski C, Gillen R, Fokin A A, Koso T V, Fokina N A, Hausmann H, Rodionov V N, Schreiner P R, Thomsen C and Maultzsch J 2017 *J. Phys. Chem. C* **121** 27082
[47] Schutte W J, De Boer J L and Jellinek F 1987 *J. Solid State Chem.* **70** 207
[48] Kumar D, Singh B, Kumar P, Balakrishnan V and Kumar P 2019 *J. Phys.: Condens. Matter'* **31** 505403
[49] Thomas A, Vikram K, Muthu D V S and Sood A K 2021 *Solid State Commun.* **336** 114412
[50] Baron A Q R 2015 arXiv:1504.01098
[51] Baron A Q R 2009 *J. Spectrosc. Soc. Japan* **58** 205–14 (arXiv:0910.5764)
[52] Bosak A, Chernyshov D, Wehinger B, Winkler B, Tacon M L and Krisch M 2015 *J. Phys. D: Appl. Phys.* **48** 504003
[53] Cai Q, Wei B, Sun Q, Said A H and Li C 2022 *Mater. Today Phys.* **28** 100856
[54] Gu X and Yang R 2014 *Appl. Phys. Lett.* **105** 131903
[55] Ribeiro-Soares J, Almeida R M, Barros E B, Araujo P T, Dresselhaus M S, Cançado L G and Jorio A 2014 *Phys. Rev. B* **90** 115438
[56] Wirtz L and Rubio A 2004 *Solid State Commun.* **131** 141
[57] Liang L, Zhang J, Sumpter B G, Tan Q-H, Tan P-H and Meunier V 2017 *ACS Nano* **11** 11777
[58] Carrete J, Li W, Lindsay L, Broido D A, Gallego L J and Mingo N 2016 *Mater. Res. Lett.* **4** 204
[59] Mohr M, Maultzsch J, Dobardžić E, Reich S, Milošević I, Damnjanović M, Bosak A, Krisch M and Thomsen C 2007 *Phys. Rev. B* **76** 035439
[60] Al Taleb A, Yu H K, Anemone G, Farías D and Wodtke A M 2015 *Carbon* **95** 731
[61] Eder S D, Hellner S K, Forti S, Nordbotten J M, Manson J R, Coletti C and Holst B 2021 *Phys. Rev. Lett.* **127** 266102
[62] Menéndez-Proupin E, Morell E S, Marques G E and Trallero-Giner C 2024 *RSC Adv.* **14** 5234
[63] Pei S, Wang Z and Xia J 2022 *Mater. Des.* **213** 110363
[64] Nayak A P, Yuan Z, Cao B, Liu J, Wu J, Moran S T, Li T, Akinwande D, Jin C and Lin J-F 2015 *ACS Nano* **9** 9117
[65] Jin Z, Li X, Mullen J T and Kim K W 2014 *Phys. Rev. B* **90** 045422
[66] Rey S I, Cross M J, Welsch M L, Schröder F, Zhou B, Stenger N, Jepsen P U and Kelleher E J R 2025 (arXiv:2503.21520)
[67] Van Troeye B, Torrent M and Gonze X 2016 *Phys. Rev. B* **93** 144304
[68] Li X, Do S-H, Yan J, McGuire M A, Granroth G E, Mu S, Berlijn T, Cooper V R, Christianson A D and Lindsay L 2022 *Acta Mater.* **241** 118390
[69] Wang Z, Selbach S M and Grande T 2014 *RSC Adv.* **4** 4069
[70] Murphy B M, Müller M, Stettner J, Requardt H, Serrano J, Krisch M and Press W 2008 *J. Phys.: Condens. Matter* **20** 224001
[71] Chaney D *et al* 2021 *Phys. Rev. Mater.* **5** 035004